The Lipoamide Dehydrogenase from *Mycobacterium tuberculosis* Permits the Direct Observation of Flavin Intermediates in Catalysis†

Argyrides Argyrou,‡ John S. Blanchard,*,‡ and Bruce A. Palfey||

Department of Biochemistry, Albert Einstein College of Medicine, 1300 Morris Park Avenue, Bronx, New York 10461, and Department of Biological Chemistry, The University of Michigan, Ann Arbor, Michigan 48109

Received May 23, 2002; Revised Manuscript Received September 17, 2002

ABSTRACT: Lipoamide dehydrogenase catalyses the NAD^+-dependent oxidation of the dihydrolipoyl cofactors that are covalently attached to the acyltransferase components of the pyruvate dehydrogenase, α-ketoglutarate dehydrogenase, and glycine reductase multienzyme complexes. It contains a tightly, but noncovalently, bound FAD and a redox-active disulfide, which cycle between the oxidized and reduced forms during catalysis. The mechanism of reduction of the *Mycobacterium tuberculosis* lipoamide dehydrogenase by NADH and [4S-^{2}H]-NADH was studied anaerobically at 4 °C and pH 7.5 by stopped-flow spectrophotometry. Three phases of enzyme reduction were observed. The first phase, characterized by a decrease in absorbance at 400−500 nm and an increase in absorbance at 550−700 nm, was fast (k_{for} = 1260 s^{-1}, k_{rev} = 590 s^{-1}) and represents the formation of $FADH_2{\cdot}NAD^+$, an intermediate that has never been observed before in any wild-type lipoamide dehydrogenase. A primary deuterium kinetic isotope effect [$^D(k_{for} + k_{rev}) \sim 4.2$] was observed on this phase. The second phase, characterized by regain of the absorbance at 400−500 nm, loss of the 550−700 nm absorbance, and gain of 500−550 nm absorbance, was slower (k_{obs} = 200 s^{-1}). This phase represents the intramolecular transfer of electrons from $FADH_2$ to the redox-active disulfide to generate the anaerobically stable two-electron reduced enzyme, EH_2. The third phase, characterized by a decrease in absorbance at 400−550 nm, represents the formation of the four-electron reduced form of the enzyme, EH_4. The observed rate constant for this phase showed a decreasing NADH concentration dependence, and results from the slow (k_{for} = 57 s^{-1}, k_{rev} = 128 s^{-1}) isomerization of EH_2 or slow release of NAD^+ before rapid NADH binding and reaction to form EH_4. The mechanism of oxidation of EH_2 by NAD^+ was also investigated under the same conditions. The 530 nm charge-transfer absorbance of EH_2 shifted to 600 nm upon NAD^+ binding in the dead time of mixing of the stopped-flow instrument and represents formation of the $EH_2{\cdot}NAD^+$ complex. This was followed by two phases. The first phase (k_{obs} = 750 s^{-1}), characterized by a small decrease in absorbance at 435 and 458 nm, probably represents limited accumulation of $FADH_2{\cdot}NAD^+$. The second phase was characterized by an increase in absorbance at 435 and 458 nm and a decrease in absorbance at 530 and 670 nm. The observed rate constant that describes this phase of ∼115 s^{-1} probably represents the overall rate of formation of E_{ox} and NADH from EH_2 and NAD^+, and is largely determined by the slower rates of the coupled sequence of reactions preceding flavin oxidation.

Lipoamide dehydrogenase (NADH:lipoamide oxidoreductase, EC 1.8.1.4)[1] is a member of the flavoprotein disulfide reductase family of enzymes (*1*) that includes glutathione reductase, trypanothione reductase, mercuric ion reductase, and the recently described *Mycobacterium tuberculosis* mycothione reductase (*2*, *3*). Lipoamide dehydrogenase is the E3 component of the pyruvate dehydrogenase, α-ketoglutarate dehydrogenase, and glycine reductase multienzyme complexes (*4*). In vivo, it catalyzes the NAD^+-dependent oxidation of the dihydrolipoyl cofactors that are covalently linked to the acyltransferase (E2) components of these multienzyme complexes. Lipoamide dehydrogenases are homodimers containing one tightly bound molecule of FAD and a redox-active disulfide per monomer. The redox-active disulfide is formed between two cysteine residues (Cys_{41} and Cys_{46}) located near the N-terminus of the polypeptide chain.

The chemical mechanism of lipoamide dehydrogenase has been determined in significant detail (*1*, *5*−*9*). In the reductive half-reaction (Scheme 1), NADH binds to the oxidized enzyme (E_{ox}) and reduces the FAD to form a transiently reduced flavin ($FADH_2$) intermediate. Internal electron transfer to the redox-active disulfide, which is thought to proceed via a covalent adduct between Cys_{46} and

† Supported by NIH Grant GM33449. B.A.P. was supported by NIH Grants GM20877 to David P. Ballou and GM11106 to Vincent Massey.

* Corresponding author. E-mail: blanchar@aecom.yu.edu. Phone: (718) 430-3096. Fax: (718) 430-8565.

‡ Albert Einstein College of Medicine.

|| The University of Michigan.

[1] Abbreviations: ATP, adenosine 5′-triphosphate; Cys_{41} and Cys_{46}, N- and C-terminal cysteine residues comprising the redox-active disulfide where the numbering refers to the *M. tuberculosis* lipoamide dehydrogenase sequence; E_{ox}, oxidized lipoamide dehydrogenase; EH_2, two-electron reduced lipoamide dehydrogenase; EH_4, four-electron reduced lipoamide dehydrogenase; FAD, flavin adenine dinucleotide; HEPES, *N*-(2-hydroxyethyl)piperazine-*N*′-(2-ethanesulfonic acid); Lip-$(S)_2$, oxidized lipoamide; Lip$(SH)_2$, reduced lipoamide; NADH, *β*-nicotinamide adenine dinucleotide (reduced form); NAD^+, *β*-nicotinamide adenine dinucleotide (oxidized form).

10.1021/bi020376k CCC: $22.00
Published on Web 11/13/2002

Scheme 1: Reductive Half-Reaction of Lipoamide Dehydrogenase

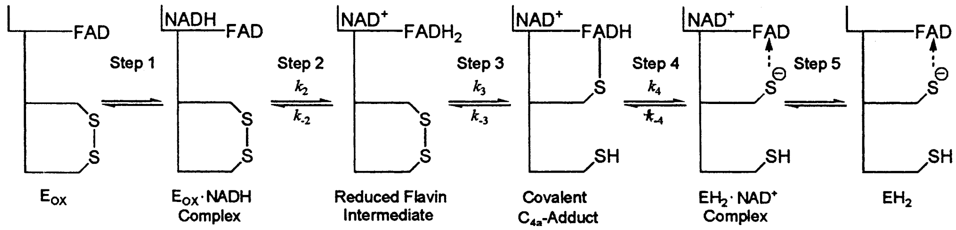

Scheme 2: Oxidative Half-Reaction of Lipoamide Dehydrogenase

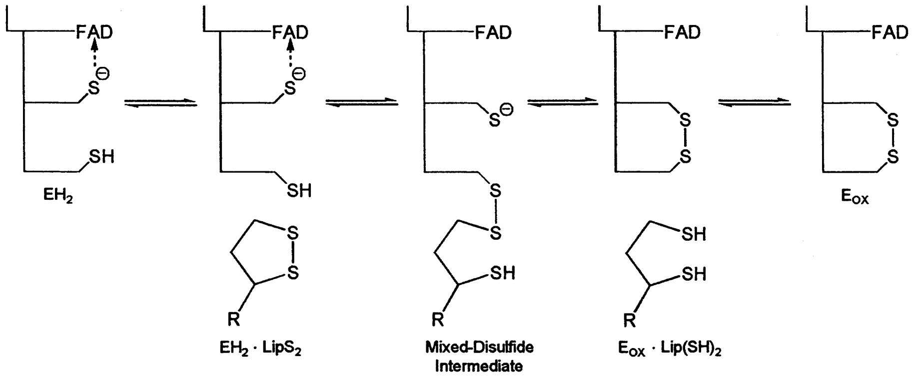

the C_{4a} position of the FAD (*1*, *6*), then generates the anaerobically stable, two-electron reduced form of the enzyme (EH_2) where the flavin is reoxidized (FAD) and the disulfide is reduced. Departure of NAD^+ completes the reductive half-reaction.

In the oxidative half-reaction (Scheme 2), the substrate lipoamide binds to the EH_2 form of the enzyme, and Cys_{41} forms a mixed disulfide with the substrate. The free thiolate of Cys_{46} then attacks the mixed disulfide to form dihydrolipoamide and to regenerate E_{ox}. This reaction is general-acid catalyzed by the essential and conserved His−Glu pair located at the C-terminus of the adjacent monomer of the homodimeric enzyme. Release of dihydrolipoamide completes the oxidative half-reaction for another round of catalysis.

Though it is known that the oxidative half-reaction is slower than the reductive half-reaction (*5*), the rate-limiting steps within each half-reaction are not known. For the reductive half-reaction, the transiently reduced flavin intermediate and the covalent C_{4a}-flavin adduct are presumed to exist, but they have never been observed before in any wild-type lipoamide dehydrogenase primarily because of the intrinsic kinetic instability of these intermediates. Therefore, it is not known whether steps leading to the formation of these intermediates or their subsequent decay are rate-limiting.

We have recently cloned, overexpressed, purified, and performed an initial characterization of lipoamide dehydrogenase from *M. tuberculosis* (*10*). The enzyme reaction is slower than previously characterized lipoamide dehydrogenases, and thus, we reasoned that direct observation of the above intermediates and perhaps other intermediates would be feasible. In this paper, we describe the results of pre-steady-state kinetics for reaction of (1) E_{ox} with NADH and [4S-^{2}H]-NADH, and (2) EH_2 with NAD^+. We observe spectroscopically, for the first time, the reduced flavin intermediate. We also show that the covalent C_{4a}-flavin adduct, which we think exists, does not accumulate significantly either in the forward or the reverse directions, suggesting that it is highly unstable. Finally, we demonstrate the thermodynamically unfavorable formation of EH_4 at high concentrations of NADH.

EXPERIMENTAL PROCEDURES

Materials. All chemicals were of analytical or reagent grade and were used without further purification unless otherwise stated. NADH, NAD^+, ATP, glucose-6-phosphate dehydrogenase from *Leuconostoc mesenteroides* (type XXIV), and yeast hexokinase (type C-300), were from Sigma. D-Glucose-l-*d* (97 at. % D) was from Aldrich.

General Methods. The enzyme concentration was determined using $\epsilon_{458nm} = 11\,300$ M^{-1} cm^{-1}. Absorbance spectra were obtained on a Hewlett-Packard 8452A diode array spectrophotometer or a Shimadzu UV-2501PC scanning spectrophotometer. Stopped-flow experiments were carried out on a Hi-Tech SF-61 DX2 instrument at 4 °C. Solutions of enzyme for rapid reaction studies were made anaerobic in glass tonometers by repeated cycles of evacuation and equilibration over an atmosphere of purified argon. Solutions of substrates for rapid reaction studies were made anaerobic by bubbling with purified argon within the syringes that were to be loaded onto the stopped-flow instrument. EH_2 was prepared by titrating anaerobic enzyme with dithionite in a tonometer equipped with a sidearm cuvette and an attached gastight syringe containing the dithionite. Formation of EH_2 was determined spectrophotometrically.

Enzyme and [4S-^{2}H]-NADH. Recombinant *M. tuberculosis* lipoamide dehydrogenase was purified as described previously (*10*). [4S-^{2}H]-NADH was prepared and purified as described previously (*11*, *12*). Fractions from the Mono-Q column (Amersham-Pharmacia Biotech) with absorbance ratios $A_{260nm}/A_{340nm} \leq 2.3$ containing [4S-^{2}H]-NADH were pooled.

Transient-State Kinetics. Stopped-flow experiments were carried out using 20 μM (refers to [FAD]) *M. tuberculosis*

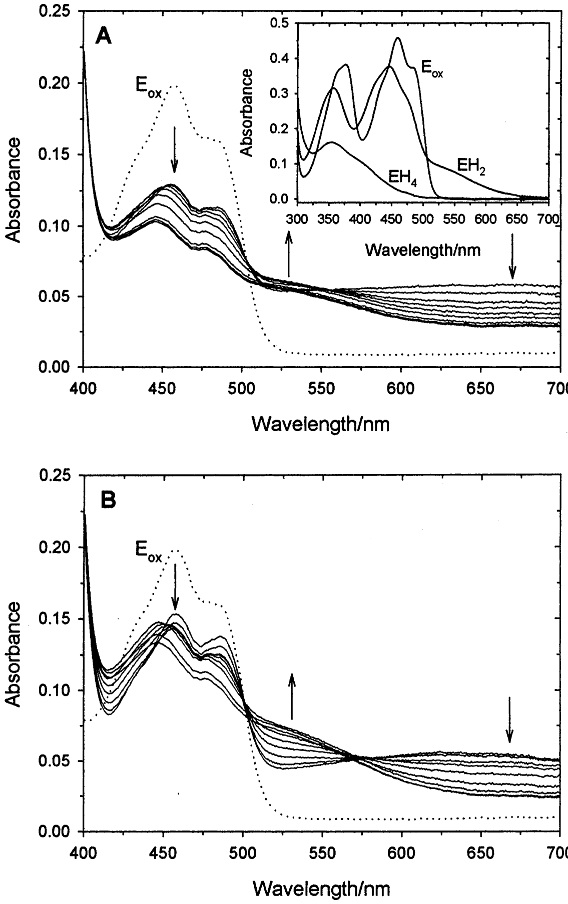

FIGURE 1: Stopped-flow absorbance traces after mixing 20 μM *M. tuberculosis* E_{ox} with 2 mM NADH (panel A) or 2 mM [4S-^{2}H]-NADH (panel B) at 4 °C and pH 7.5. The dotted spectrum is that of 20 μM E_{ox}. The solid spectra were recorded using a diode-array detector 2.2, 3.7, 6.7, 9.7, 14.2, 21.7, 39.7, 210, and 1400 ms after mixing. The arrows indicate increasing time. The spectra in the inset of Figure 1A were obtained from the anaerobic reduction of the enzyme using a catalytic amount of NAD^+ in the presence of glucose-6-phosphate and glucose-6-phosphate dehydrogenase. Spectra were scanned frequently over the course of the reaction, and the spectra of EH_2 and EH_4 were calculated using a three-component singular value decomposition analysis implemented in the program Specfit (Spectrum Software Associates).

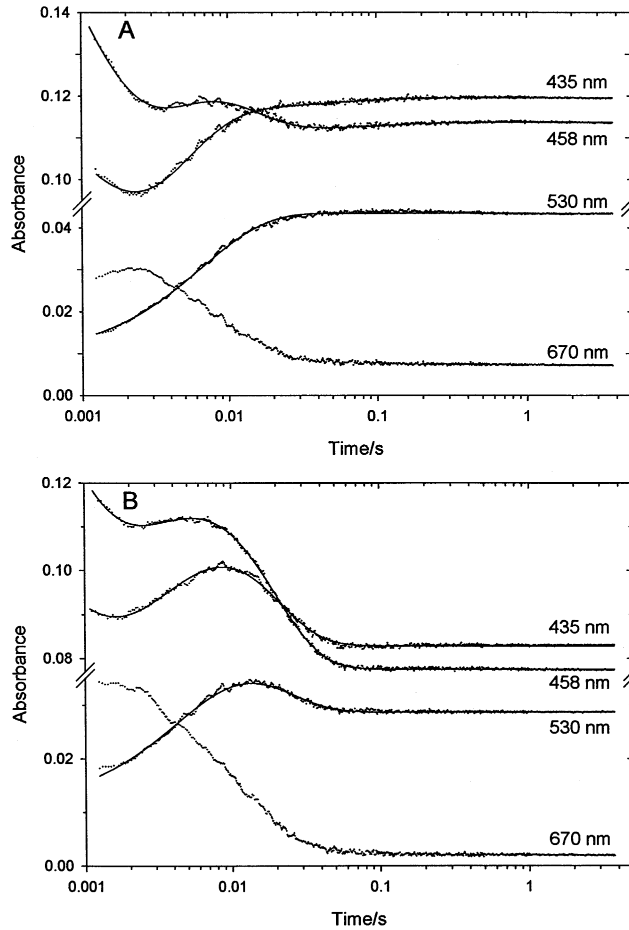

FIGURE 2: Stopped-flow absorbance traces after mixing 20 μM *M. tuberculosis* E_{ox} with 100 μM NADH (panel A) or 2 mM NADH (panel B) at 4 °C and pH 7.5 and monitored at the indicated wavelengths. The points are the experimental data, and the solid lines are the fits to eq 1. Note the logarithmic time-scales.

lipoamide dehydrogenase and $\geq$100 μM concentrations of substrates to ensure pseudo-first-order kinetics. Time courses were fit to the sum of two or more exponential functions (eq 1):

$$A_t = A_1 e^{-k_1 t} + A_2 e^{-k_2 t} + A_3 e^{-k_3 t} + c \qquad (1)$$

where A_t is the absorbance at time, t, A_1–A_3 are the amplitudes of the phases of reaction described by the observed pseudo-first-order rate constants, k_1–k_3, and c is a constant.

Reduction Potentials and Estimation of EH_2 levels at Equilibrium. The reduction potentials of the E_{ox}/EH_2 and EH_2/EH_4 redox couples were determined spectrophotometrically at 25 °C in 100 mM sodium phosphate buffer, pH 7.0, by the xanthine/xanthine oxidase method of Massey (*13*), using benzyl viologen ($E_{m7} = -359$ mV) and safranin O ($E_{m7} = -289$ mV) as redox indicator dyes. To estimate the levels of EH_2 at equilibrium, we used the final absorbances at the end of the reactions of E_{ox} with NADH from the stopped-flow experiments and the determined extinction coefficients (ϵ) of the unliganded forms of EH_2 and EH_4 (Figure 1A, inset). We used these values to calculate a $\Delta\epsilon$ ($\epsilon_{EH_2} - \epsilon_{EH_4}$) at 435 nm ($\Delta\epsilon = 7645$ M^{-1} cm^{-1}) and 458 nm ($\Delta\epsilon = 7903$ M^{-1} cm^{-1}) to determine the amount of EH_2 at equilibrium. We note that the values obtained in this way are estimates because at least some of the EH_2 and EH_4 forms of the enzyme are likely to be bound with pyridine nucleotide, which can change their extinction coefficient.

RESULTS

Spectral Properties of the M. tuberculosis Lipoamide Dehydrogenase E_{ox}, EH_2, and EH_4 Enzyme Species. Figure 1 A (inset) shows the spectral properties of the three ligand-free anaerobically stable species of *M. tuberculosis* lipoamide dehydrogenase. The oxidized enzyme (E_{ox}) has absorbance maxima at 375 and 458 nm, a shoulder at ~485 nm, and minima at 308 and 403 nm. In the two-electron reduced enzyme (EH_2), the flavin remains oxidized while the redox-active disulfide is reduced. The absorbance is attenuated, and the maxima are blue-shifted relative to those in E_{ox}, and absorbance appears at longer wavelengths with a shoulder at ~530 nm previously attributed to a Cys_{46}–thiolate FAD charge-transfer interaction. In the four-electron reduced enzyme (EH_4), the absorbance maxima are further decreased, and the 530 nm Cys_{46}–thiolate FAD charge-transfer absor-

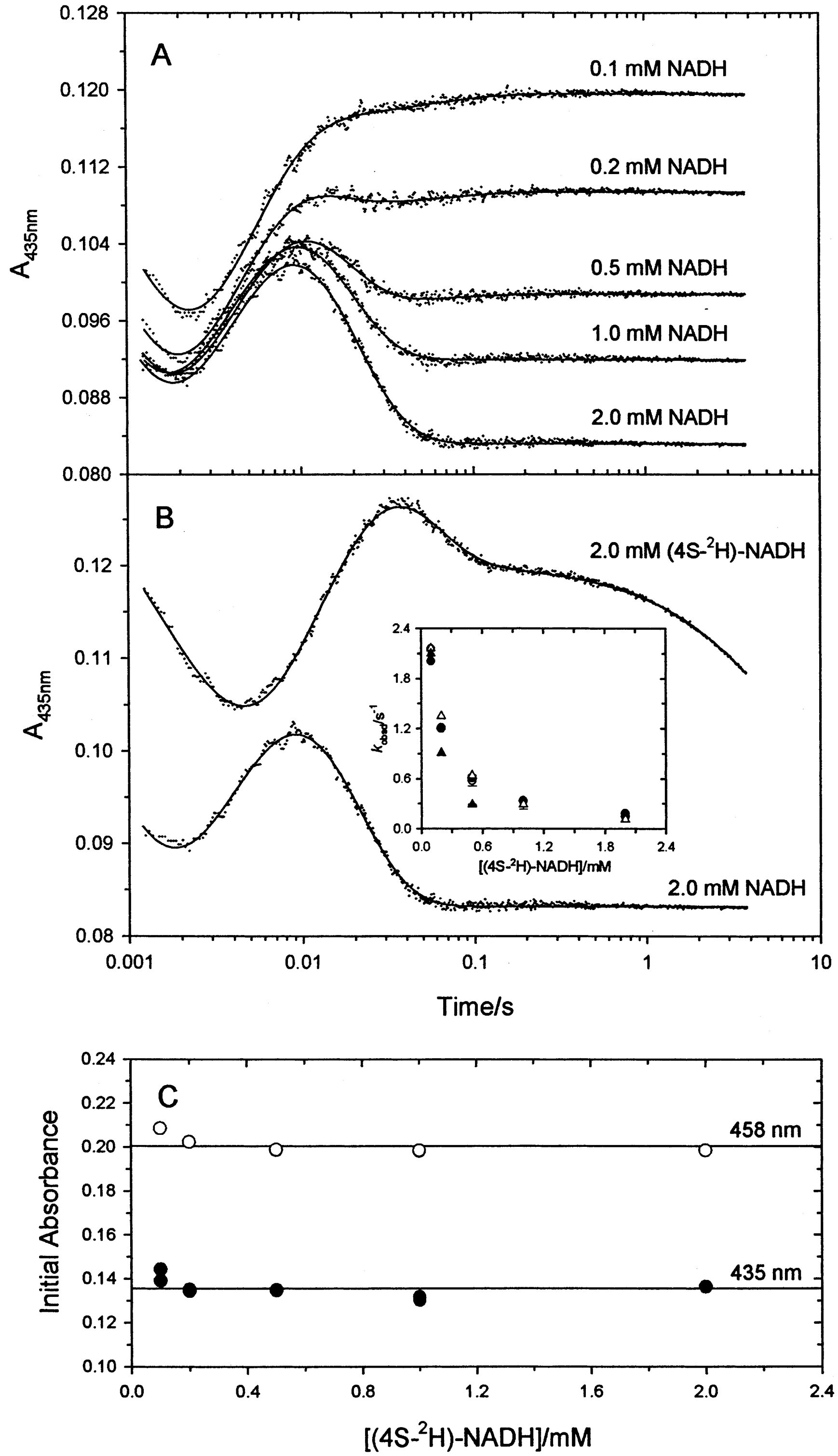

FIGURE 3: (A) Stopped-flow absorbance traces after mixing 20 μM *M. tuberculosis* E_{ox} with the indicated [NADH] at 4 °C and pH 7.5 and monitored at 435 nm, to illustrate thermodynamically unfavorable formation of EH_4. Note the logarithmic time-scales. (B) Stopped-flow absorbance traces after mixing 20 μM *M. tuberculosis* E_{ox} with 2 mM NADH or 2 mM [4S-^{2}H]-NADH at 4 °C and pH 7.5 and monitored at 435 nm to illustrate a primary deuterium kinetic isotope effect on the various phases of reaction. The points are the experimental data, and the solid lines are fits to eq 1. The inset shows the dependence of k_{obs} on the concentration of [4S-^{2}H]-NADH for the fourth phase of reaction (see text). (C) Initial absorbance values at the indicated wavelengths obtained from the fits for reaction of 20 μM *M. tuberculosis* E_{ox} with [4S-^{2}H]-NADH. The solid lines are the average values of the initial absorbance.

bance disappears. The spectral properties of these three enzyme species are very similar to the spectra of the corresponding species of the pig heart lipoamide dehydrogenase (*1*). Knowledge of the spectral properties of these unliganded enzyme species is useful in interpreting the spectral properties of complexes of these species with the various substrates and products, as well as other unstable intermediate species in catalysis, which will be presented below.

Reduction of E_{ox} with NADH and [4S-^{2}H]-NADH. Figure 1 shows the spectral changes that occur as E_{ox} is mixed rapidly with NADH (panel A) or [4S-^{2}H]-NADH (panel B)

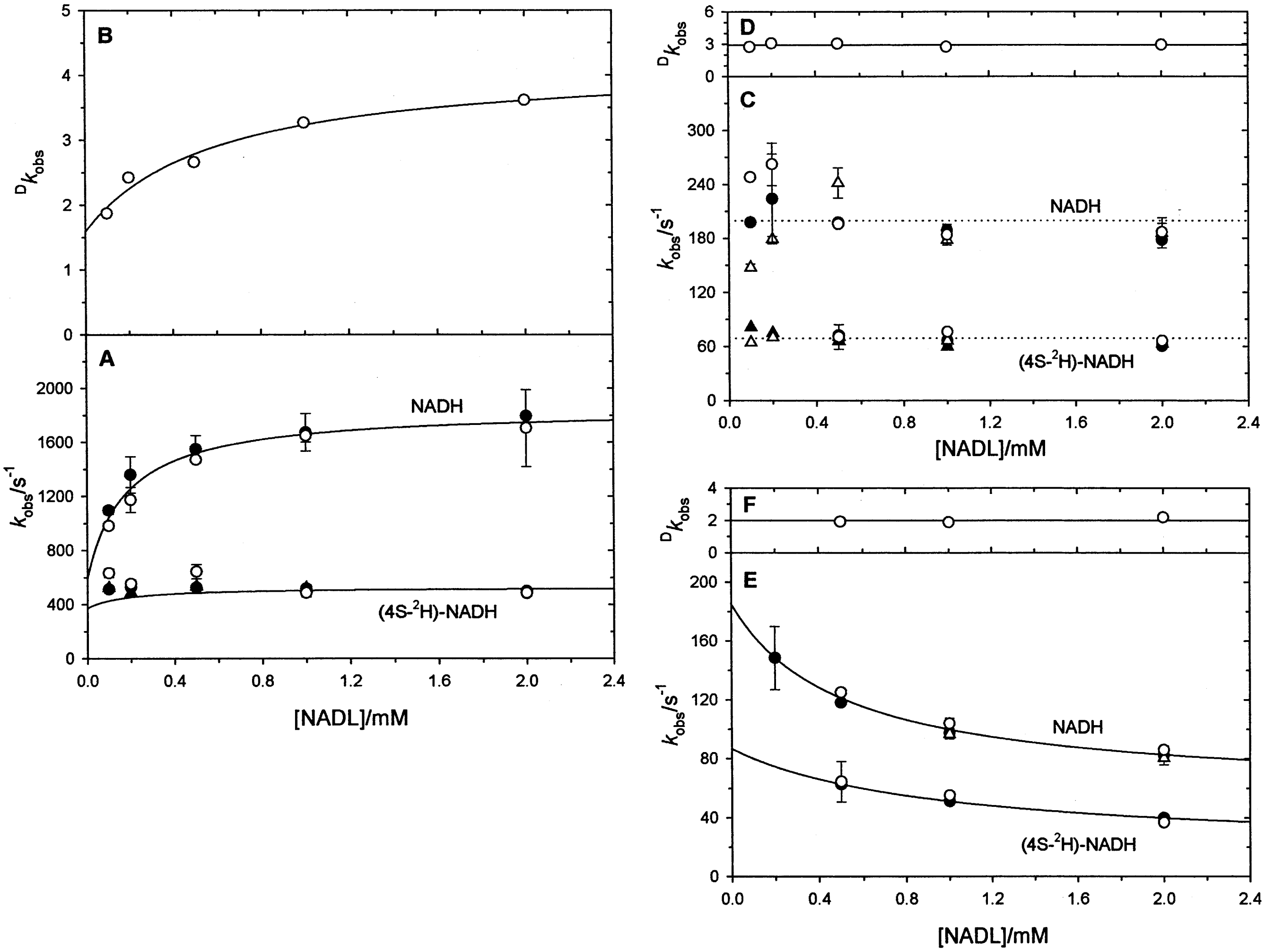

FIGURE 4: The NADL concentration dependence of k_{obs} for the first (panel A), second (panel C), and third (panel E) phase of reaction of 20 μM *M. tuberculosis* E_{ox} with NADL at 4 °C and pH 7.5. The different symbols represent fitted k_{obs} values obtained at the various wavelengths (○, 435 nm; ●, 458 nm; △, 530 nm; ▲, 670 nm). Panels B, D, and F show the primary deuterium kinetic isotope effect on k_{obs} for each phase of reaction. The solid line for the NADH data in panel A is a fit to eq 2, and the fitted parameters are shown in Table 1. The solid line through the [4S-^{2}H]-NADH data in panel A is a theoretical line described by eq 2 with values of k_2^D, k_{-2}^D, and K_D of 160 s^{-1}, 370 s^{-1}, and 180 μM, respectively (see text). The solid line through the data in panel B is a fit to eq 3 with $^{D}k_{-2} = 1.6$, $k_{max}^H/k_{max}^D = 4.2$, and $k_{-2}^D \times K_D/k_{max}^D = 0.6$. The solid lines in panel E are fits to eq 5, and the fitted parameters are shown in Table 1.

in a stopped-flow apparatus and monitored using a diode-array detector. Figure 2 shows single wavelength traces performed at low (panel A) and high (panel B) concentrations of NADH. The 435 and 458 nm traces monitor the oxidation state of the FAD, the 530 nm trace monitors the levels of EH_2, while the 670 nm trace monitors a species distinct from any of the unliganded enzyme species shown in Figure 1A (inset). Three phases of reaction are observed. The first phase is very fast and is characterized by a decrease in absorbance at 435 and 458 nm and an increase in absorbance at 670 nm. The second phase is slower and is characterized by regain of absorbance at 435 nm, gain in absorbance at 530 nm, and loss of absorbance at 670 nm. The third phase is even slower and is characterized by decreases in absorbance at 435, 458, and 530 nm.

The amplitude of this last phase is almost undetectable at low NADH concentration but becomes very prominent as the concentration of NADH is increased as shown in Figures 2B and 3A. These experiments were repeated using [4S-^{2}H]-NADH to determine the primary kinetic isotope effects on individual steps and to assist in assigning the phases. Figure 3B shows a comparison of the kinetics of reaction of E_{ox} with 2 mM NADH and [4S-^{2}H]-NADH monitored at 435 nm. The various phases of reaction are clearly slower using [4S-^{2}H]-NADH demonstrating the presence of a primary deuterium kinetic isotope effect. [4S-^{2}H]-NADH displays an additional very slow phase (Figure 3B), visible at all wavelengths (data not shown), and its origin will be addressed in the discussion. The time courses were fit to the sum of two or more exponential functions (eq 1, Experimental Procedures), and the observed rate constant of each phase (k_{obs}) was plotted as a function of the concentration of NADL[2] as shown in Figure 4. Figure 4, panels B, D, and F, also shows the apparent isotope effect ($^{D}k_{obs}$) on the first, second, and third phase of the reaction, respectively, at each concentration of NADL. These observed isotope effects were calculated by averaging k_{obs} determined at the various wavelengths and then taking the ratio, k_{aver}^H/k_{aver}^D.

[2] "L" in NADL refers to hydrogen (^{1}H) or deuterium (^{2}H).

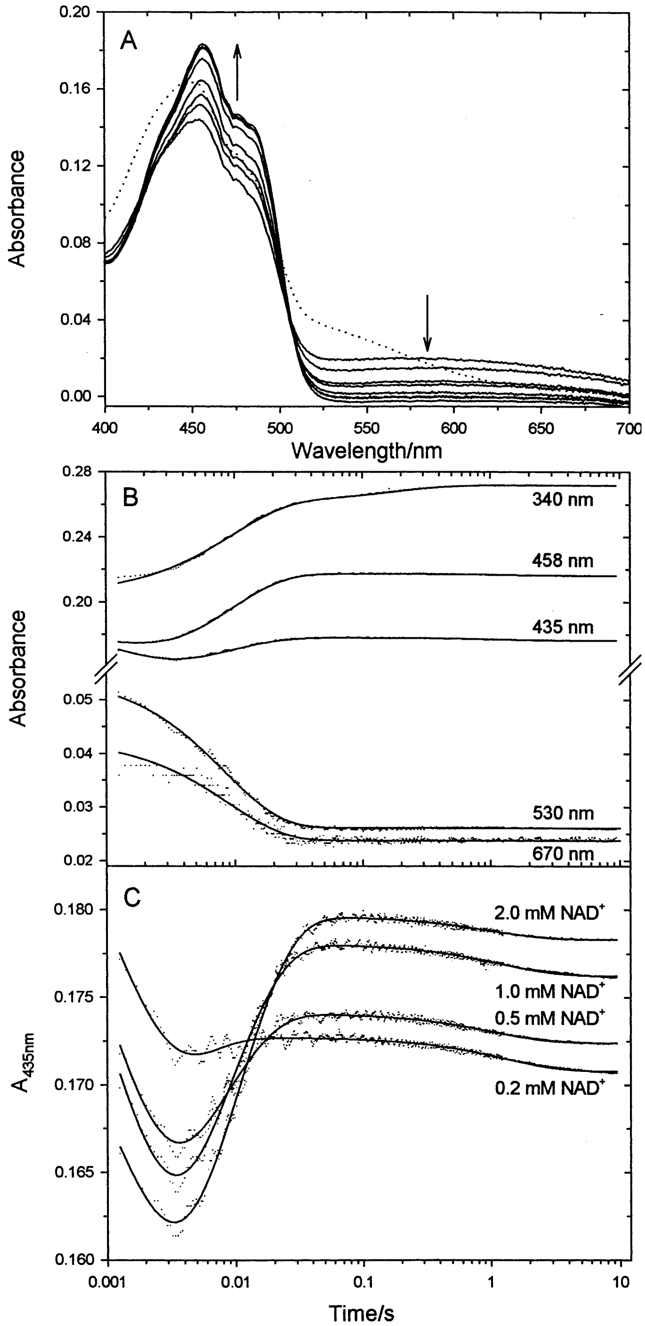

FIGURE 5: (A) Stopped-flow absorbance traces after mixing 20 μM *M. tuberculosis* EH_2 with 2 mM NAD^+ at 4 °C and pH 7.5. The dotted spectrum is that of 20 μM *M. tuberculosis* EH_2. The solid spectra were recorded using a diode-array detector 2.2, 3.7, 6.7, 9.7, 14.2, 21.7, 39.7, 210, and 1400 ms after mixing. The arrows indicate increasing time. (B) Stopped-flow absorbance traces after mixing 20 μM *M. tuberculosis* EH_2 with 1 mM NAD^+ at 4 °C and pH 7.5 and monitored at the indicated wavelengths. (C) Stopped-flow absorbance traces after mixing 20 μM *M. tuberculosis* EH_2 with the indicated [NAD^+] at 4 °C and pH 7.5 and monitored at 435 nm. The points are the experimental data and the solid lines are fits to eq 1. Note the logarithmic time-scales.

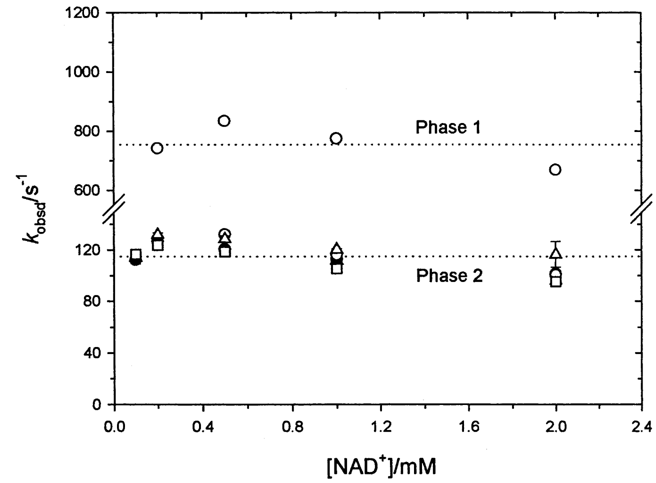

FIGURE 6: The NAD^+ concentration dependence of k_{obs} for the first and second phases of reaction of 20 μM *M. tuberculosis* EH_2 with NAD^+ at 4 °C and pH 7.5. The different symbols represent fitted k_{obs} values obtained at the various wavelengths (○, 435 nm; ●, 458 nm; △, 530 nm; ▲, 670 nm; □ 340 nm).

We estimate that, using NADH, approximately 85−90% of the first phase occurred in the dead-time of mixing. As a result, fitting of the time courses to eq 1 was difficult. With [4S-^{2}H]-NADH on the other hand, an isotope effect of ∼4.2 on the first phase permitted the observation of ∼40% of the amplitude of this phase. The initial absorbance values at 435 and 458 nm obtained from the fits are independent of the concentration of [4S-^{2}H]-NADH, and they are shown in Figure 3C. To obtain more accurate rates for the first phase of reaction of E_{ox} with NADH, we constrained the initial absorbance at 435 and 458 nm to the average values obtained from the [4S-^{2}H]-NADH data: 0.136 and 0.201, respectively. The rate constant data using NADH presented in Figure 4 were obtained by adding this constraint. We note that constraining the initial absorbance instead to the values for E_{ox} (0.170, 435 nm; 0.227, 458 nm) gave rates that were 20−25% higher for the first phase. The smaller predicted initial absorbance values used in the final fitting, rather than the corresponding values for E_{ox}, are likely due to perturbation of the E_{ox} spectrum upon binding NADL in an FAD· NADL charge-transfer complex.

Oxidation of EH_2 by NAD^+. Figure 5A shows the spectral changes that occur as EH_2 is rapidly mixed with NAD^+ in a stopped-flow apparatus and monitored using a diode-array detector. The 530 nm Cys_{46}−thiolate−FAD charge-transfer absorbance gets shifted to longer wavelengths with a maximum at ∼600 nm in the dead time of mixing. Figure 5B shows traces at 1 mM NAD^+ monitored at 340, 435, 458, 530, and 670 nm, while panel C shows traces at 435 nm as [NAD^+] is varied from 0.2 to 2 mM. Three phases are observed. The first phase, which is clearly visible as a decrease in absorbance at 435 nm, is also observed at 458 nm, though with a much smaller amplitude change. The second phase is slower and is characterized by increases in absorbance at 340, 435, and 458 nm and decreases in absorbance at 530 and 670 nm. The third phase, which is visible at all wavelengths, has a very small amplitude change, is too slow to be catalytically important, and was not further evaluated. The time courses were fit to the sum of two or three exponential functions (eq 1, Experimental Procedures) and the rate of each phase was plotted as a function of the concentration of NAD^+ as shown in Figure 6.

DISCUSSION

Direct Observation of a Reduced Flavin Intermediate. The first phase in the reaction of E_{ox} with NADH, characterized by loss of absorbance at 435 and 458 nm, is consistent with

Scheme 3

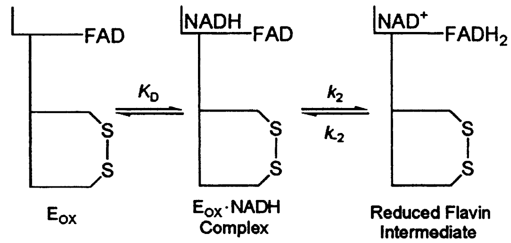

Table 1: Rate Constants for Individual Steps in the Reductive Half-Reaction of *M. tuberculosis* Lipoamide Dehydrogenase[a]

rate constant[b]	rate/ s^{-1}	isotope effect	K_D (NADH)
k_2^H	1260 ± 50	$^{D}k_2 = 8 \pm 4$	$180 + 20\ \mu M$
k_2^D	160 ± 90		
k_{-2}^H	590 ± 60	$^{D}k_{-2} = 1.6 \pm 0.3$	
k_{-2}^D	370 ± 90		
k_3[c]	200 ± 20	–	–
k_{-3}[c]	115 ± 10	–	–
k_6[d]	57 ± 2	–	–
k_{-6}[d]	128 ± 2	–	–

[a] At pH = 7.5 and 4 °C. [b] Defined in Schemes 1, 3, and 4. [c] These values are observed rate constants and are likely to include contributions from step 4 as well (see Figures 4 and 6, Schemes 1 and 5, and text). [d] These values are unlikely to be microscopic rate constants (see text).

reduction of FAD by NADH to form an $FADH_2$·NAD^+ intermediate. The loss of absorbance at 435 and 458 nm occurs at the same rate as gain of absorbance at 670 nm, and this signal may be attributed to an $FADH_2$–NAD^+ charge-transfer interaction. Though this species has never been observed before in any wild-type lipoamide dehydrogenase, it has been observed in an H450S mutant of *Azotobacter vinelandii* lipoamide dehydrogenase (*14*) and in an H450A mutant of yeast glutathione reductase (*15*). This first phase displays a primary deuterium kinetic isotope effect of ~4.2 (see below) using [4S-^{2}H]-NADH consistent with reduction of FAD by hydride/deuteride transfer from NADL.

We used the two-step binding model shown in Scheme 3 (*16*, *17*) to analyze the concentration dependence of the first phase of reaction of E_{ox} on [NADH]. In this model, E_{ox} and NADH are presumed to be in rapid equilibrium[3] with the E_{ox}·NADH complex, and the dependence of k_{obs} on the concentration of NADH can be described by eq 2 (*16*, *17*):

$$k_{obs} = k_{-2} + \frac{k_2[\mathrm{NADH}]}{K_D + [\mathrm{NADH}]} \qquad (2)$$

This equation describes a hyperbola with a maximum rate (k_{max}), at infinite concentration of NADH, of $k_2 + k_{-2}$ and a *Y*-intercept of k_{-2} (*16*, *17*). The solid line in Figure 4A is the best fit to this equation and the fitted parameters are shown in Table 1.

[3] This analysis of the first phase relies on and is simplified by rapid equilibrium binding of NADL to E_{ox}. The kinetic constants that pertain to the hydride transfer step (step 2, Scheme 1) presented in Table 1 do not apply if a more complex model involving steady-state binding of E_{ox} to NADL is operating.

Internal Electron Transfer to the Redox-Active Disulfide. The second phase in the reaction of E_{ox} with NADL is most consistent with the reoxidation of the flavin as electrons are transferred to the redox-active disulfide. The increase in absorbance at 435 and 458 nm occurs at the same rate as the loss of the 670 nm absorbance due to the loss of the $FADH_2$·NAD^+ charge transfer. The increase in 530 nm absorbance, a wavelength region characteristic of the EH_2 form of the enzyme, also occurs at the same apparent rate as flavin reoxidation and loss of the $FADH_2$·NAD^+ charge transfer interaction. Taken together, these results demonstrate that this second phase of enzyme reduction is due to intramolecular transfer of electrons from the flavin to the redox-active disulfide to ultimately generate EH_2.

Isotope Effects. The intrinsic primary deuterium kinetic isotope effect for hydride transfer from NADL to FAD ($^{D}k_2$) is obtained by taking the ratio of k_2^H to k_2^D. Likewise, the isotope effect for hydride transfer from FADHL to NAD^+ ($^{D}k_{-2}$) is obtained by taking the ratio of k_{-2}^H to k_{-2}^D. The data for the first phase of reaction of E_{ox} with [4S-^{2}H]-NADH show no concentration dependence in the experimentally attainable region (Figure 4A), and thus precludes the determination of k_2^D and k_{-2}^D by this direct graphical method. An alternative, somewhat indirect, method to obtain k_2^D and k_{-2}^D is described below.

The ratio k_{obs}^H/k_{obs}^D, which we define as $^{D}k_{obs}$, at each concentration of NADL can be fit to eq 3 (the derivation can be found in the Appendix) to obtain a value of 1.6 ± 0.3 for $^{D}k_{-2}$ and 4.2 ± 0.5 for k_{max}^H/k_{max}^D, as shown in Figure 4B. The value for k_{-2}^D of $370 \pm 90\ s^{-1}$ can then be obtained from the relationship, $k_{-2}^D = k_{-2}^H/{}^{D}k_{-2}$. Finally, the value of $160 \pm 90\ s^{-1}$ for k_2^D can then be obtained from eq 4:

$$^{D}k_{obs} = {}^{D}k_{-2} + \frac{\left(\dfrac{k_{max}^H}{k_{max}^D} - {}^{D}k_{-2}\right)[\mathrm{NADH}]}{\left(\dfrac{k_{-2}^D}{k_{max}^D} K_D + [\mathrm{NADH}]\right)} \qquad (3)$$

$$k_{max}{}^{D} = k_2^D + k_{-2}^D = 530 \pm 20\ s^{-1} \qquad (4)$$

The solid line drawn through the [4S-^{2}H]-NADH data (Figure 4A) is a theoretical curve described by eq 2 with values of k_2^D, k_{-2}^D, and K_D of 160 s^{-1}, 370 s^{-1}, and 180 μM, respectively. The fact that k_{obs} shows no apparent dependence on the concentration of [4S-^{2}H]-NADH (Figure 4A) can now be rationalized as resulting from a high value of k_{-2}^D relative to k_2^D.

The above values for k_2^D and k_{-2}^D were then used, in conjunction with k_2^H and k_{-2}^H, to calculate the intrinsic primary deuterium kinetic isotope effects, $^{D}k_2$ and $^{D}k_{-2}$ (Table 1). The calculated values for these isotope effects of 8 ± 4 and 1.6 ± 0.3 for $^{D}k_2$ and $^{D}k_{-2}$, respectively, are in the normal range expected from semiclassical behavior. Their ratio of 5.0 ± 3.4 which defines the equilibrium isotope effect, $^{D}K_{eq} = {}^{D}k_2/{}^{D}k_{-2}$, is somewhat difficult to interpret due to the large error. The error sets the lower limit to 1.6, a value that is an upper limit for equilibrium isotope effects. Values of 5, however, are significantly higher than normal and could perhaps be explained as follows. The above analysis assumes that exchange of the deuterium atom, which resides on N_5 of the reduced FAD after deuteride transfer, with protons of nearby residues is significantly slower than back reaction to regenerate [4S-^{2}H]-NADH and E_{ox}. The extent to which this is true will govern the magnitude of $^Dk_{-2}$ and, therefore, the magnitude of $^DK_{eq}$. If the deuterium exchange rate becomes significant, the measured rate of the back reaction will be larger than the true value of k_{-2}^{D} because it will be contaminated to some extent by k_{-2}^{H}. As a result, the measured $^Dk_{-2}$ and $^DK_{eq}$ values will be smaller and larger than the true values, respectively. A conserved lysine residue (Lys_{50} in the *M. tuberculosis* lipoamide dehydrogenase) is within hydrogen bonding distance of N_5 of the flavin of the closely related *Pseudomonas putida* lipoamide dehydrogenase (*18*) and is a potential source of three protons for which the N_5-D of the reduced flavin might exchange.

Finally, the magnitude of the isotope effect on k_{max} decreases from a value of 4.2 for the first phase to values of 2.9 and 2.0 for the second and third phases of reaction, respectively (Figure 4, panels B, D, and F). Observed isotope effects are often smaller than the intrinsic value due to kinetic complexity. The fact that the reduced flavin intermediate ($FADH_2 \cdot NAD^+$) accumulates in solution in the direction of FAD reduction by NADH is strong evidence that step(s) after hydride transfer are rate-limiting, and these steps contribute to the kinetic complexity of the system resulting in the incremental decrease of the observed isotope effect as the reaction progresses from one phase of reaction to the next.

EH_4 Formation. The result of the above two phases of reaction of E_{ox} with NADL is the formation of the two-electron reduced enzyme (EH_2), where the flavin is oxidized and the redox-active disulfide is reduced. Further reduction to the four-electron reduced state (EH_4) requires that the flavin also be reduced (Figure 1A, inset). The observed third phase of reaction of E_{ox} with NADL is characterized by decreases in absorbance at 435 and 458 nm, consistent with a second round of flavin reduction. At the same rate, 530 nm absorbance is lost signaling the disappearance of EH_2, and consistent with formation of EH_4 during this third phase of reaction.

Formation of EH_4 shows a decreasing NADL concentration dependence of k_{obs} (Figure 4E). This behavior is interpreted in the context of a two-step reaction, where the first step is slow and the second NADH-binding step, as well as subsequent steps, are fast (*19*, *20*). The first step may be the slow release of NAD^+ before rapid binding and reaction with NADL as shown in Scheme 4, although slow isomerization of EH_2 to another ionic form of EH_2, or a conformational change are also possible. Equation 5 describes this behavior (*19*, *20*):

Scheme 4

$$EH_2{\cdot}NAD^+ \underset{k_{-6}}{\overset{NAD^+ \;\; k_6}{\rightleftharpoons}} EH_2 \underset{K_D}{\overset{NADH}{\rightleftharpoons}} EH_2{\cdot}NADH \overset{NAD^+}{\rightleftharpoons} EH_4$$

$$k_{obs} = k_6 + \frac{k_{-6}K_D}{K_D + [NADH]} \qquad (5)$$

It can be seen that when the concentration of NADH is high, k_{obs} tends toward k_6. Similarly, as the concentration of NADH approaches zero, k_{obs} approaches $k_6 + k_{-6}$, thus explaining the decreasing rate as the concentration of NADH increases. This analysis assumes complete formation of $EH_2 \cdot NAD^+$ at the end of the second phase. However, the observed rate constants for the second and third phases (Table 1) are not sufficiently different for this to be a valid assumption. As a result, the values of k_6 and k_{-6} obtained from the above analysis are unlikely to be microscopic rate constants, but instead represent net rate constants. The solid lines in Figure 4E are the fits to eq 5 and the rate constants are tabulated in Table 1. Though EH_4 does form, its rate of formation cannot be obtained from these experiments because the rate of formation of EH_2, a required intermediate leading to formation of EH_4, is slower and hence makes subsequent fast steps kinetically invisible.

Reaction of E_{ox} with [4S-^{2}H]-NADH shows an additional very slow phase (Figure 3B), which is not observed with NADH and must, therefore, be related to the nature of isotopic substitution. We propose that this last phase results from a combination of (1) an equilibrium isotope effect and (2) eventual washout of deuterium from [4S-^{2}H]-NADH into solvent. Deuterium could wash out by exchanging with solvent from N_5 of the reduced flavin, followed by reoxidation of the flavin by NAD^+ and release of NADH. In separate experiments (not shown), the absorbance at 435 nm for [4S-^{2}H]-NADH eventually reaches the same value for NADH, an observation consistent with our deuterium washout proposal. Also consistent with our proposal is the pronounced decreasing [4S-^{2}H]-NADH concentration dependence of k_{obs} for this last phase (inset in Figure 3B). For example, 20 μM enzyme active sites will require five complete rounds of flavin reduction and reoxidation to completely convert 100 μM [4S-^{2}H]-NADH to NADH (assuming no deuterium internal return), but 100 complete rounds of flavin reduction and reoxidation to completely convert 2 mM [4S-^{2}H]-NADH to NADH, thus the decreasing concentration dependence.

A Highly Unstable Covalent C_{4a}-Flavin Adduct. Intramolecular transfer of electrons from the reduced flavin to the disulfide to generate EH_2 is thought to proceed via a covalent C_{4a}-flavin adduct (*1*, *6*). Covalent C_{4a}-flavin adducts are characterized by absorbance maxima at ~380 nm (*21*). No significant increase in absorbance at 380 nm was observed in the reaction of E_{ox} with NADH (data not shown), suggesting that the covalent C_{4a}-flavin adduct does not accumulate significantly in the forward direction.

To determine whether the covalent C_{4a}-flavin adduct accumulates in the reverse direction, oxidation of EH_2 by NAD^+, we generated EH_2 by anaerobic titration of E_{ox} with dithionite and rapidly mixed this form of the enzyme with NAD^+ in a stopped-flow apparatus. The 530 nm charge-transfer shoulder, which is characteristic of the unliganded form of EH_2 (Figure 1A, inset), shifted to ~600 nm in the mixing dead-time of the instrument (Figure 5, panels A and B). We attribute this spectroscopic signal to an $EH_2 \cdot NAD^+$ complex. A similar spectral shift was observed when NAD^+ was titrated with the EH_2 form of lipoamide dehydrogenase from pig heart (*9*). The predicted initial absorbance at 530 nm obtained from the fits of the corresponding time courses (data not shown) decreases in a titratable manner with increasing [NAD^+]. We used these data to obtain an estimate of the K_D for NAD^+ of ~130 μM.

After this rapid binding, the absorbance at 435 nm decreases transiently (Figure 5C), indicating flavin reduction. The absorbance at 458 nm also decreases (Figure 5B), although with a smaller change in amplitude. The two species that might accumulate to some extent and be responsible for this phase are the covalent C_{4a}-flavin adduct and the reduced flavin intermediate ($FADH_2 \cdot NAD^+$), since they are both characterized by diminished absorbance in this wavelength region. However, we think that it is the reduced flavin intermediate that more likely accumulates rather than the covalent C_{4a}-flavin adduct because no significant increase at ~380 nm was observed during this phase (data not shown).

When the amount of intermediate that accumulates during a reaction is very small, as is in the present case (see Figure 5), one has to be cautious in the assignment of an observed rate constant that describes a certain phase to a specific step in a reaction. For example, in the reaction sequence, A → B → C, if the intermediate, B, decays faster than it is formed, (i) it will only accumulate at low levels, and (ii) it will appear to form with its decomposition rate constant and decay with its formation rate constant (*22*)! Given that the reduced flavin intermediate accumulates to low levels in this reverse reaction and that the observed rate constant describing the first phase of ~750 s^{-1} is similar in magnitude to k_{-2}^{H} (590 s^{-1}, Table 1), we think that this rate represents the rate of oxidation of the reduced flavin intermediate by NAD^+ to form E_{ox} and NADH.

The observed rate constant describing this phase of ~750 s^{-1} shows no NAD^+ concentration dependence in the experimentally attainable region (Figure 6), even though the K_D for NAD^+ is large enough that an increase in rate should have been observed. We think the estimates of these rates are perhaps not precise enough to clearly see the increase, a consequence of the small amplitude of this phase in conjunction with the fact that a large portion of this phase occurred in the mixing dead time.

The second slower phase of reaction is characterized by regain in absorbance at 435 and 458 nm and is consistent with formation of E_{ox} (Figure 5, panels B and C). An increase in absorbance at 340 nm (Figure 5B and Figure 6, squares), representing the formation of NADH, occurs at the same rate. We think that the observed rate constant that describes this phase of ~115 s^{-1} represents the overall rate of formation of E_{ox} and NADH from EH_2 and NAD^+ and is largely determined by the slower rates of the coupled sequence of reactions preceding flavin oxidation.

The amplitude of this second phase increases with increasing [NAD^+] even though the rate does not appear to change. This apparent contradiction may be reconciled if E_{ox} binds NAD^+. This would act as a sink so that more and more of the products (E_{ox}, $E_{ox} \cdot NAD^+$, and NADH) are formed in the final equilibrium. The cocrystal structure of the *Pseudomonas putida* lipoamide dehydrogenase bound to NAD^+ is evidence for an $E_{ox} \cdot NAD^+$ complex in these enzymes (*18*).

In summary, the covalent C_{4a}-flavin adduct does not appear to accumulate to a significant extent either in the forward (E_{ox} plus NADH) or in the reverse (EH_2 plus NAD^+) directions, suggesting that it is highly unstable. This instability could arise if formation of this intermediate in either direction is considerably slower than its decay in either direction.

Table 2: Comparison of the Reduction Potentials of Lipoamide Dehydrogenases from *E. coli,* Pig Heart, and *M. tuberculosis*[a]

organism	E_{ox}/EH_2 (mV)	EH_2/EH_4 (mV)
E. coli[b]	−264	−317
pig heart[c]	−280	−346
M. tuberculosis	−309	−382

[a] At pH 7.0. [b] Ref *7*. [c] Ref *8*.

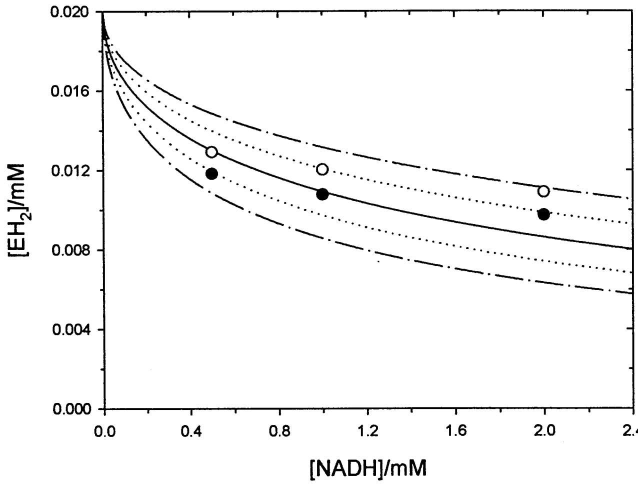

FIGURE 7: Equilibrium concentrations of EH_2 after reaction of 20 μM *M. tuberculosis* lipoamide dehydrogenase and increasing concentrations of NADH to illustrate a good correlation between theoretical (lines) and observed (○, 435 nm; ●, 458 nm) equilibrium EH_2 levels. The solid line was generated from the experimentally determined value of the reduction potential for the EH_2/EH_4 couple of −382 mV, while the dotted and dashed−dotted lines are deviations of ±5 and ±10 mV from this value, respectively.

Formation of EH_4 is Thermodynamically Unfavorable. The absorbance end-points for the 435 and 458 nm time courses in the reaction of E_{ox} with NADH (Figures 2 and 3A) are well above zero, indicating that a considerable amount of oxidized FAD remains. This remaining absorbance titrates with increasing concentration of NADH (Figure 3A) and suggests that the reduction potential for the EH_2/EH_4 couple is significantly more negative than that of the NADH/NAD^+ couple, making reduction of EH_2 to EH_4 by NADH thermodynamically unfavorable. To test this hypothesis, we determined the reduction potentials for the E_{ox}/EH_2 and EH_2/EH_4 redox couples for the *M. tuberculosis* lipoamide dehydrogenase using the xanthine/xanthine oxidase method of Massey (Table 2) (*13*).

From these reduction potentials (−309 and −382 mV, respectively) and the known reduction potential for NADH (−320 mV), one can calculate equilibrium constants (K_{eq}') for the following reactions:

$$E_{ox} + NADH \xrightleftharpoons{K_{eq}' = 2.36} EH_2 + NAD^+$$

$$EH_2 + NADH \xrightleftharpoons{K_{eq}' = 0.0080} EH_4 + NAD^+$$

Using these equilibrium constants, the equilibrium concentrations of EH_2, NADH, EH_4, and NAD^+ can be determined from known starting concentrations of E_{ox} (20

Scheme 5: Chemical and Kinetic Mechanism for the Reductive Half-Reaction of *Mycobacterium tuberculosis* Lipoamide Dehydrogenase at 4 °C and pH 7.5

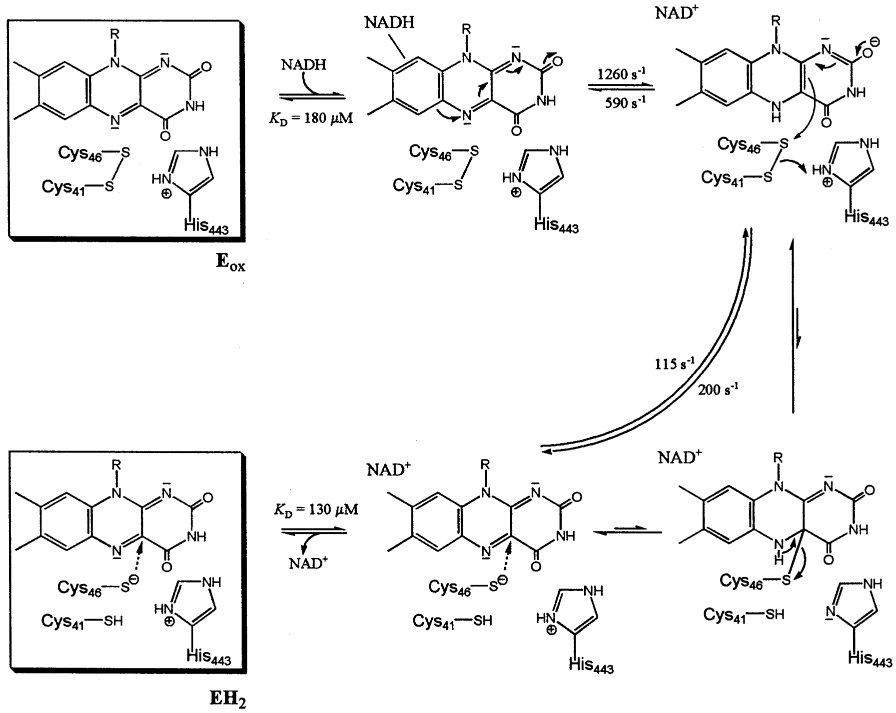

μM) and various levels of NADH. Figure 7 shows the calculated equilibrium concentration of EH_2 at various levels of NADH (solid line). Also shown in Figure 7 are calculated equilibrium concentrations of EH_2 for EH_2/EH_4 reduction potentials of ±5 (dotted lines) and ±10 mV (dashed−dotted lines) of the experimentally determined value of −382 mV. There are two assumptions that are used in this calculation: (1) that there is no E_{ox} at any level of NADH; though this is not true at low [NADH], at [NADH] $\geq$0.5 mM there are negligible amounts of E_{ox} remaining ($\leq$1.7%); and (2) that the reduction potential for this couple is not influenced by bound pyridine nucleotide and vice versa.

The end-points of the reaction of E_{ox} with NADH were used to estimate the amount of EH_2 at equilibrium (Experimental Procedures) shown in Figure 7 (○, 435 nm; ●, 458 nm). We emphasize that these values are estimates because, at least some of the EH_2 and EH_4 forms of the enzyme are likely to be bound by pyridine nucleotide, which can change their extinction coefficient. Nevertheless, there is a good correlation between calculated and measured levels of EH_2 at equilibrium, and it appears that thermodynamically unfavorable formation of EH_4 by NADH is sufficient to account for incomplete reduction of the flavin cofactor even at levels of NADH (2 mM) that are 100 times that of the enzyme (20 μM).

Finally, comparison of the reduction potentials for the two redox couples of lipoamide dehydrogenases from *E. coli* (*7*), pig heart (8), and *M. tuberculosis* shows that the *M. tuberculosis* enzyme has the most negative E_{ox}/EH_2 and EH_2/EH_4 redox couples. This is perhaps one reason the *M. tuberculosis* lipoamide dehydrogenase is relatively slow, and thus permits the direct observation of the above-mentioned flavin intermediates in catalysis.

CONCLUSIONS

We have analyzed the observed multi-phasic time courses for reaction of *M. tuberculosis* lipoamide dehydrogenase E_{ox} with NADL, and EH_2 with NAD^+, and have assigned the various phases of reaction to the formation and decay of intermediates that have previously been observed in wild-type, mutant (*14*), or chemically modified (*6*) lipoamide dehydrogenases from various species. We present a chemical and kinetic model for the reductive half-reaction of *M. tuberculosis* lipoamide dehydrogenase (Scheme 5) that accommodates our findings. NADH binds to E_{ox} and reduces the FAD by transferring the *C4-proS* hydride of the dihydronicotinamide ring to N_5 of the flavin. Hydride transfer is fast (k_{for} = 1260 s^{-1} and k_{rev} = 590 s^{-1}) and displays a primary deuterium kinetic isotope effect [$^{D}(k_{for} + k_{rev})$] of ~4.2. The result is the formation of a transiently reduced flavin intermediate that accumulates in solution because a subsequent step leading to formation of EH_2 is slow (k_{obs} = 200 s^{-1}). The high instability of the covalent C_{4a}-flavin adduct limits its accumulation to levels that make it undetectable during the process of intramolecular transfer of electrons from the reduced flavin to the disulfide. NAD^+ release completes the reductive half-reaction.

ACKNOWLEDGMENT

We thank Professors David P. Ballou and Vincent Massey, University of Michigan, for the generous use of their facilities and Professor Charles H. Williams, Jr., University of Michigan, for a critical reading of the manuscript. We also thank the reviewers for their insightful comments and suggestions. We dedicate this work to the late Professor Vincent Massey, whose work on lipoamide dehydrogenase, more than forty years ago, made intepretation of the present work possible.

APPENDIX

Derivation of eq 3:

$$k_{obs} = k_{-2} + \frac{k_2[S]}{K_D + [S]} \tag{2}$$

$$k_{obs} = \frac{k_{-2}(K_D + [S]) + k_2[S]}{K_D + [S]}$$

$$k_{obs} = \frac{k_{-2}K_D + (k_2 + k_{-2})[S]}{K_D + [S]}$$

$$k_{obs} = \frac{k_{-2}K_D + k_{max}[S]}{K_D + [S]}$$

$$\frac{k^H_{obs}}{k^D_{obs}} = \frac{k^H_{-2}\,K_D + k^H_{max}\,[S]}{k^D_{-2}K_D + k^D_{max}\,[S]}$$

Multiply and divide the $k^H_{-2}\,K_D$ term by k^D_{-2}:

$$\frac{k^H_{obs}}{k^D_{obs}} = \frac{k^H_{-2}\,\dfrac{k^D_{-2}}{k^D_{-2}}\,K_D + k^H_{max}\,[S]}{k^D_{-2}K_D + k^D_{max}\,[S]}$$

$$\frac{k^H_{obs}}{k^D_{obs}} = \frac{{}^Dk_{-2}\;k^D_{-2}\,K_D + k^H_{max}\,[S]}{k^D_{-2}\,K_D + k^D_{max}\,[S]}$$

Divide throughout by k^D_{max}:

$$\frac{k^H_{obs}}{k^D_{obs}} = \frac{{}^Dk_{-2}\,\dfrac{k^D_{-2}}{k^D_{max}}\,K_D + \dfrac{k^H_{max}}{k^D_{max}}\,[S]}{\dfrac{k^D_{-2}}{k^D_{max}}\,K_D + [S]}$$

Add and subtract the term, ${}^Dk_{-2}\,[S]$, to the numerator:

$$\frac{k^H_{obs}}{k^D_{obs}} = \frac{{}^Dk_{-2}\,\dfrac{k^D_{-2}}{k^D_{max}}\,K_D + \dfrac{k^H_{max}}{k^D_{max}}\,[S] + {}^Dk_{-2}[S] - {}^Dk_{-2}[S]}{\dfrac{k^D_{-2}}{k^D_{max}}\,K_D + [S]}$$

Collect terms:

$$\frac{k^H_{obs}}{k^D_{obs}} = \frac{{}^Dk_{-2}\left(\dfrac{k^D_{-2}}{k^D_{max}}\,K_D + [S]\right) + \left(\dfrac{k^H_{max}}{k^D_{max}} - {}^Dk_{-2}\right)[S]}{\left(\dfrac{k^D_{-2}}{k^D_{max}}\,K_D + [S]\right)}$$

Finally, carry out the division of both terms in the numerator:

$$\frac{k^H_{obs}}{k^D_{obs}} = {}^Dk_{-2} + \frac{\left(\dfrac{k^H_{max}}{k^D_{max}} - {}^Dk_{-2}\right)[S]}{\left(\dfrac{k^D_{-2}}{k^D_{max}}\,K_D + [S]\right)} \tag{3}$$

REFERENCES

1. Williams, C. H., Jr. (1992) in *Chemistry and Biochemistry of Flavoenzymes* (Muller, F., Ed.) pp 121−211, CRC Press, Boca Raton.
2. Patel, M. P., and Blanchard, J. S. (1999) *Biochemistry 38,* 11827−11833.
3. Patel, M. P., and Blanchard, J. S. (2001) *Biochemistry 40,* 5119−5126.
4. Reed, L. J. (1974) *Acc. Chem. Res. 7,* 40−46.
5. Massey, V., Gibson, Q. H., and Veeger, C. (1960) *Biochem. J. 77,* 341−351.
6. Thorpe, C., and Williams, C. H., Jr. (1981) *Biochemistry 20,* 1507−1513.
7. Wilkinson, K. D., and Williams, C. H., Jr. (1979) *J. Biol. Chem. 254,* 852−862.
8. Matthews, R. G., and Williams, C. H., Jr. (1976) *J. Biol. Chem. 251,* 3956−3964.
9. Matthews, R. G., Ballou, D. P., and Williams, C. H., Jr. (1979) *J. Biol. Chem. 254,* 4974−4981.
10. Argyrou, A., and Blanchard, J. S. (2001) *Biochemistry 40,* 11353−11363.
11. Ottolina, G., Riva, S., Carrea, G., Danieli, B., and Buckmann, A. F. (1989) *Biochim. Biophys. Acta 998,* 173−178.
12. Orr, G., and Blanchard, J. S. (1984) *Anal. Biochem. 142,* 232−234.
13. Massey, V. (1991) *Flavins and Flavoproteins*, pp 59−66, Walter de Gruyter & Co., Berlin.
14. Benen, J., van Berkel, W., Dieteren, N., Arscott, D., Williams, C., Veeger, C., and de Kok, A. (1992) *Eur. J. Biochem. 207,* 487−497.
15. Rietveld, P., Arscott, L. D., Berry, A., Scrutton, N. S., Deonarian, M. P., Perham, R. N., and Willams, C. H., Jr. (1994) *Biochemistry 33,* 13888−13895.
16. Johnson, K. A. (1986) *Methods Enzymol. 134*, 677−705.
17. Strickland, S., Palmer, G., and Massey, V. (1975) *J. Biol. Chem. 250,* 4048−4052.
18. Mattevi, A., Obmolova, G., Sokatch, J. R., Betzel, C., and Hol, W. G. (1992) *Proteins 13,* 336−351.
19. Fersht, A. (1985) *Enzyme Structure and Mechanism*, pp 136−137, W. H. Freeman and Company, New York.
20. Schopfer, L. M., Massey, V., and Nishino, T (1988) *J. Biol. Chem. 263,* 13528−13538.
21. Ghisla, S., Entsch, B., Massey, V., and Husein, M. (1977) *Eur. J. Biochem. 76,* 139−148.
22. Fersht, A. (1985) *Enzyme Structure and Mechanism*, pp 133−134, W. H. Freeman and Company, New York.

BI020376K